A sodium-dependent communication pathway across class A G-protein coupled receptors

Neil J. Thomson[1], **Owen N. Vickery**[1,2], **Callum M. Ives**[1], **and Ulrich Zachariae**[1,✉]

[1]Computational Biology, School of Life Sciences, University of Dundee, Dundee DD1 5EH, UK.,
[2]Current address: School of Life Sciences, University of Warwick, Coventry CV4 7AL, UK.

G-protein-coupled receptors (GPCRs) are membrane proteins that transmit signals across the cell membrane by activating intracellular effector proteins in response to extracellular ligand interaction. A large majority of GPCRs are characterized by an evolutionarily conserved activation mechanism, involving the reorientation of helices and residue side chains, rearrangement of an internal hydrogen bonding network, and the expulsion of a sodium ion from an ionizable binding site in the transmembrane region. However, how sodium, internal water, and protein residues interplay to determine the overall receptor state remains elusive. Here, we employed information theory to trace signal transmission pathways through the receptors and identify their concerted response to sodium binding and protonation. Applying our methodology, 'State Specific Information', to all-atom molecular dynamics simulations of pharmaceutically important GPCRs, we discovered a conserved communication pathway that enabled the exchange of information between the sodium binding site and the distal G-protein binding region, connecting the most highly conserved ionizable residues in the receptors. Reorientation of internal water molecules was essential for the coupling of conformational state changes of protein residues along this pathway, which ultimately reconfigured the conformation of the G-protein binding site. The presence of sodium disconnected this pathway. By inhibiting protonation, sodium was found to serve as a master switch that determined the molecular state of GPCRs during the receptors' transition to activation.

Correspondence: ***u.zachariae@dundee.ac.uk***

Introduction

G-protein coupled receptors (GPCRs) form the largest superfamily of cell surface receptors with over 800 members that control a broad range of physiological processes. GPCRs span the plasma membrane of the cell from the extracellular to the intracellular face and act as signal transducers that enable transmembrane communication between the outside and inside of the cell. Ligand interaction on the extracellular domain induces conformational changes that expose binding sites on the intracellular face, initiating intracellular signalling by binding various effector proteins including heterotrimeric G-proteins and β-arrestins, each of which cause different physiological changes (1). As such, GPCRs form the main target for drug therapies, with over 30% of US food and drug administration (FDA) approved drugs targeting about 108 different GPCRs (2).

Class A receptors comprise the vast majority of GPCRs with over 700 members. High-resolution crystal structures of inactive class A GPCRs resolve a sodium ion (Na^+) bound to a highly conserved, ionizable residue central to the transmembrane (TM) domain (residue $Asp^{2.50}$ - Ballesteros-Weinstein numbering system). However, this ion is not present in active state crystal structures, implicating the ion in GPCR activation (3–8). Computational studies show that the absence of sodium triggers protonation of $Asp^{2.50}$, and protons and ionizable networks are thought to be involved in GPCR signaling (4, 9–12). In addition, the presence of a conserved network of internal water molecules connecting polar residues, including $Asp^{2.50}$, likely plays an important role in GPCR signal transduction (13). Through molecular dynamics simulations of a range of class A GPCRs, Venkatakrishnan *et al*. reveal the presence of well-defined water pockets that are conserved across both active and inactive states and further, state-dependent water sites (14). Upon activation, a significant re-positioning of the TM water-network seems to be coupled to the collapse of the (Na^+) binding pocket, although the functional significance of these waters is unclear (14–16).

Various studies correlate GPCR activation with transitions between distinct rotameric conformations of evolutionarily conserved residues, termed microswitches. It is believed that these rotamer transitions underpin the large scale conformational changes that govern activation (1, 15, 17–24). Many microswitches form distinct motifs, such as the CWxP motif at the ligand binding site, which is known to link directly to the sodium ion binding pocket (8). The conformation of the P-I-F motif is also strongly coupled to ligand binding (24). The $NPxxY^{7.53}$ motif is located proximal to the ion binding site and includes $Tyr^{7.53}$, which opens and closes a transmembrane water channel according to simulation studies (10, 16). In addition, the ionizable DRY motif at the intracellular face plays a key role in G-protein binding, and forms ionic locks that maintain the inactive receptor state (1, 21) (Fig. 1). These observations suggest that the ion binding site, water mediated interactions, and conserved residues are critical for G-protein signalling. However so far, the functional interaction of these components remains unknown (8, 14, 25).

GPCR signal transduction is a process whereby information is sent, encoded, transmitted and received, in parallel with the tenets of an information system (26). Therefore, Na^+, internal water, and microswitches can be seen to act as essential components of an information system. To resolve their role in enabling receptor movements leading to activation, we developed a methodology termed "State Specific Information" (SSI), which combines Shannon's mutual information (26, 27) and McGill's interaction information (also called co-information) (28–31). SSI quantifies how much information, specific to a certain residue or cofactor state, is shared between coupled transitions in these networks. Con-

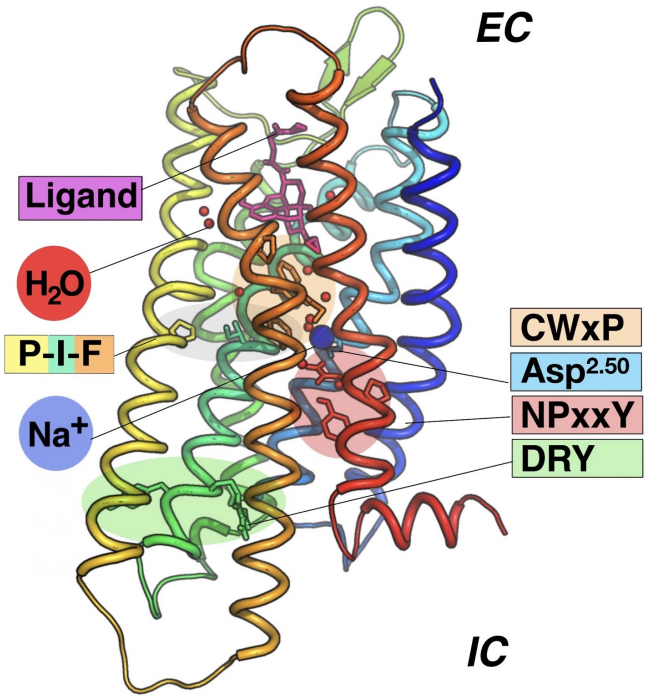

Fig. 1. Class A GPCR key features. The ligand binding pocket, internal waters, sodium ion (Na^+), conserved microswitch motifs, and primary sodium binding residue $Asp^{2.50}$ in the μ-opioid receptor (pdb: 4dkl). EC, extracellular and IC, intracellular side.

trasting correlation approaches that calculate mutual information using residue or atom covariance (4, 30, 32–35), SSI is closely aligned with the concept of microswitches by requiring residues to have at least two conformational states to exchange any information. Thereby, we extracted information from large-scale, persistent changes between interlinked residue states that can be traced back to a specific cause, such as the binding of Na^+. In the case of water molecules, transferred information was calculated based on pocket occupancy as well as water orientation.

We conducted all-atom molecular dynamics simulations initiated from three inactive-state, antagonist-bound class A GPCRs: the A_{2A}-adenosine receptor ($A_{2A}AR$), the μ-opioid receptor (μOR), and the δ-opioid receptor (δOR). For each receptor, we collected simulation data on 1.7 μs timescales performed in three different receptor states of the main ion binding residue: $Asp^{2.50}$ in a charged state with sodium bound (Na^+/D^-), $Asp^{2.50}$ in a charged state with sodium removed ($0/D^-$), and $Asp^{2.50}$ in a protonated state without sodium ($0/D^n$). Receptor transitions caused by expelling sodium, and subsequently protonating $Asp^{2.50}$, were represented by concatenating trajectory pairs. This way, each process corresponds to 1 bit of information (e.g. 'protonated or de-protonated') termed "information source". SSI for each information source was then calculated between 7875 residue and internal water pairs. Focusing on information transferred through residue side chain movements (35), we investigated the effects in the side chain dihedral angles of all Ballesteros-Weinstein positions common to all three receptors from the intracellular face to the base of the orthosteric pocket, including the CWxP motif, totaling 121 residues.

Our results revealed how sodium, $Asp^{2.50}$-protonation, and internal water molecules are coupled to protein microswitch conformations, forming a long-range information transfer pathway between two highly conserved ionizable regions - $Asp^{2.50}$ and the DRY motif at the G-protein binding site. By determining receptor protonation, sodium was found to act as the master switch turning on and off communication with the G-protein binding interface at the intracellular side.

Results

Sodium unbinding and protonation at $Asp^{2.50}$ forms an information pathway to the intracellular DRY motif. Five water pockets, local to receptor regions of highly conserved motifs and residues, exhibited large probability densities for receptor-internal water molecules in all three receptor simulations (Fig. 2A,C). Four of these water sites are conserved in class A GPCRs (14). To determine whether these five water sites acted as information transfer routes, they were investigated in addition to the 121 protein residues.

Rather than affecting the entire protein, information specific to the ion binding state of $Asp^{2.50}$ (SSI) was shared between a small group of key microswitch and water site pairs, both for sodium and protonation ($\sim$ 5% and 6%, respectively). Within this small number of affected microswitches, our analysis revealed long-range information transfer sent from the ion binding site to the P-I-F motif, the NPxxY motif, and the distal ionizable DRY motif involved in the G-protein binding interface (Fig. 2B). For example, the conformation of residue $Arg^{3.50}$ of the $DR^{3.50}Y$ motif, at a distance of $\sim$22 Å, was strongly impacted by $Asp^{2.50}$-protonation (Fig. 2B).

We found that internal water molecules acted as important players in transmitting information emerging from the ion binding site. The states of these water molecules were more indicative of the ion binding states of $Asp^{2.50}$ than the majority of the protein residues (Fig. 2B). These results suggest that water molecules are an integral part of the signal transmission mechanism, and that the internal waters therefore represent additional elements of an extended set of microswitches. Furthermore, Water 1 (Wat1) is known to form water-mediated interactions present in the inactive receptor state, while interactions with water 2 (Wat2) are correlated with the active receptor state (14). In parallel with this, protonation of $Asp^{2.50}$ decreased the occupancy of the Wat1 site by $\sim$25%, whereas the Wat2 water site showed an increased occupancy by $\sim$25% in this state.

The magnitude of information exchanged within the three receptors after sodium expulsion and $Asp^{2.50}$-protonation was projected onto the μOR crystal structure in Fig. 2C. For both causes, the SSI values revealed a pathway that included water and transmitted information between $Asp^{2.50}$ and the DRY motif by propagating conformational changes along helix 7 and across the receptor base. The tight connectivity of coupled transitions on this pathway ultimately allowed changes at $Asp^{2.50}$ to affect the conformation of the distal G-protein binding site. This way, it established coupling between ionizable residues at long range ($Asp^{2.50}$, $Asp^{3.49}$, and $Arg^{3.50}$), whose ability to change protonation state is recognized as a

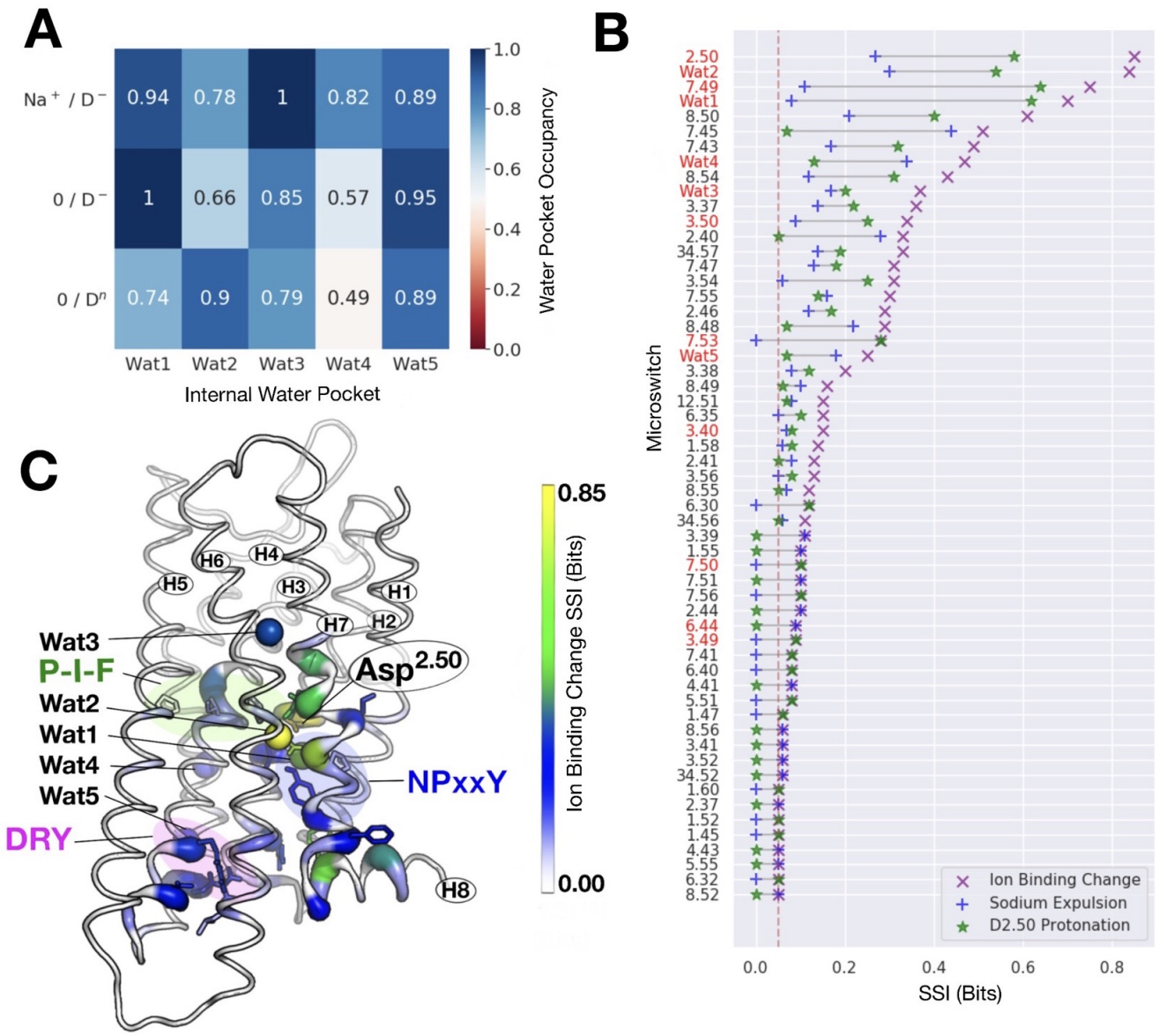

Fig. 2. State Specific Information reveals information flow propagating through the receptor. **(A)** Water pocket occupancy averaged across all three receptors throughout the simulations; a value of 1 reflects complete occupancy in all receptors over the entire simulated time. **(B)** SSI is passed on from the information source to protein microswitches and internal water molecules. Shown are all significant SSI values in bits, shared between both information sources (sodium expulsion and $Asp^{2.50}$-protonation: 1 bit each) and each microswitch. High SSI values reflect microswitches that have a highly specific conformational state preference for each of the $Asp^{2.50}$ ion binding states. Both information sources uniquely alter the presence and orientation of all five investigated internal water molecules (Wat1-Wat5) as well as having a long-range impact on the conformational state of the DRY motif. The significance threshold is depicted by a vertical red dashed line (0.05 bits), internal water and key residues and motifs are highlighted in red. **(C)** SSI values (bits) representing information flow of $Asp^{2.50}$ ion binding changes projected as colour-code (from white, 0 bits to yellow, 0.85 bits) onto the μOR crystal structure (pdb:4dkl). Key microswitches are shown as sticks, water molecules as spheres. Microswitches involved in SSI transfer form a pathway bridging the ion binding site and the DRY motif at the G-protein binding site. Information is transmitted as conformational changes along this pathway to the intracellular face.

hallmark of class A GPCR activation (13). Following protonation of $Asp^{2.50}$, the conformational change at $Arg^{3.50}$ also impacted the conformation of residue 6.30 (the helix 6 ionic lock), and position 34.57 on intracellular loop 2 (ICL2), known to play a role in effector protein binding specificity and bias. Since SSI is symmetric, note that the identified information pathway could also serve to support information flow from the DRY motif toward the ion binding site, caused for instance by the intracellular binding of G-proteins or other effectors.

$Asp^{2.50}$-protonation couples to water molecules for efficient information transfer. Two key motifs implied in receptor activation, NPxxY and DRY, shared SSI only upon $Asp^{2.50}$-protonation (Figs. 2B and S1; for full SSI data see Supplementary Information). Unlike sodium expulsion, $Asp^{2.50}$-protonation caused all residues of the $NP^{7.50}xxY$ motif, including $Pro^{7.50}$, to undergo various degrees of conformational rearrangement. Structurally, $Asp^{2.50}$-protonation promoted a conformational change to $Pro^{7.50}$, and altered the conformation of the hydrophobic barrier created by $Tyr^{7.53}$ (10) (Fig. 3A). In addition, SSI indicated that protonation strongly impacted Wat1 and Wat2, both of which acted as

primary microswitches for the transmission of information.

To study the functional role of the internal water network in greater detail, we employed interaction or co-information (co-SSI) (28–31) to quantify the effect of intercalated water molecules Wat1-Wat5 on information transfer between the $Asp^{2.50}$ ion binding site and all microswitches. Positive co-SSI indicated that the coupling between each microswitch and the ion binding site was stabilised by their interaction with water molecules, amplifying their shared SSI. In accordance with the results from LeVine & Weinstein (30), negative co-information was interpreted as destabilisation of microswitch conformations, induced by interacting with water molecules, attenuating their shared information.

As shown by co-SSI, the water network had a particularly pronounced effect on the information pathway upon $Asp^{2.50}$-protonation (Fig. 3A,B). Specifically, co-SSI values demonstrated that the conformations of Wat1 and Wat2 adopted in the $Asp^{2.50}$-protonated state substantially contributed to stabilising the conformational reorientation along the pathway to the G-protein binding site. The reorientation of Wat1, in particular, was responsible for the majority of SSI shared between the protonation site and the NPxxY and DRY motifs (Fig. 3B).

This showed that rearrangement of Wat1 and Wat2 was essential for triggering conformational changes coupled to $Asp^{2.50}$-protonation throughout the receptor, including the establishment of communication between the NPxxY and DRY motifs. The negative value of co-SSI between $Pro^{7.50}$, Wat1, and $Asp^{2.50}$-protonation as the information source, by contrast, implied that Wat1 destabilised the conformational state of $Pro^{7.50}$ upon $Asp^{2.50}$-protonation, which may contribute to the kinking of helix 7 seen upon activation (for full co-SSI data see Supplementary Information).

Molecular mechanism of information transfer from the ion binding site. To elucidate the molecular mechanism of information transfer propagating from the ion binding site, we analysed the nature of the conformational changes induced by $Asp^{2.50}$-protonation across the receptors. In our simulations of both deprotonated states (Na^+/D^- and $0/D^-$), it was observed that near the ion binding site, the side chain oxygen of $Asp^{2.50}$ acted as a H-bond acceptor for Wat1, mediating a bond with $Asn^{1.50}$ and $Tyr^{7.53}$, whose OH group pointed towards the Wat1 pocket in all three receptors (Fig. 3C).

$Asp^{2.50}$-protonation triggered substantial rearrangements in its neighborhood in all three receptor types. The altered H-bonding pattern induced a change to the rotamer state of Wat1, while simultaneously, $Tyr^{7.53}$ rotated its OH group away from the Wat1 pocket (Fig. 3C). Furthermore, the water bridge between $Asp^{2.50}$ and $Tyr^{7.53}$ was disrupted upon $Asp^{2.50}$ protonation. Thereby, $Tyr^{7.53}$ flipped into its downward state (a movement previously shown to correlate with opening a hydrophobic gate (10, 16)) in the protonated $A_{2A}AR$ and μOR. In the δOR the same transition was observed upon further protonation of $Asp^{3.49}$. This residue forms part of the $D^{3.49}RY$ motif and is coupled to $Asp^{2.50}$-protonation by the information pathway.

Our co-SSI analysis indicated that reorientation of Wat1 was essential for allowing $Tyr^{7.53}$ to adopt a new conformation. The protonation-dependent downward movement of $Tyr^{7.53}$ ultimately triggered the conformational change of the DRY motif, as demonstrated by the SSI shared between these microswitches. In the μOR, this conformational rearrangement was an upward swing of $Arg^{3.50}$ into its active, G-protein binding conformation (Fig. 3C). In addition, the inter-hydroxyl distance between $Tyr^{7.53}$ and $Tyr^{5.58}$ was reduced in the μOR and $A_{2A}AR$. In the μOR, $Asp^{2.50}$-protonation was sufficient to decrease the $Tyr^{7.53}$-$Tyr^{5.58}$ inter-hydroxyl distance to the distribution seen in the active state, when compared to data from a 1.7-μs simulation of the active crystal structure (pdb: 6ddf) (Fig. S3). We also found that the G-protein binding cavity opened upon further protonation of $Asp^{3.49}$ in the δOR, as measured by the TM2-TM6 activation coordinate between $Thr^{2.39}$-Cα and $Ile^{6.33}$-Cα (Fig. S4), indicating a role of protonating conserved residues in activation.

Sodium restrains key microswitches to a single conformation. The sodium-bound form of class A GPCRs is associated with their inactive state (5, 8, 10, 36). Around the sodium binding site, $Asp^{2.50}$, $Tyr^{7.53}$ and $Asn^{1.50}$ (a 100% conserved residue in class A GPCRs), three residues known to form a hydrogen bonding triplet with Wat1, were restrained to highly ordered single conformations in all three sodium-bound receptors. This was reflected by their zero conformational state entropies (see Methods) (Fig. 4). The water-mediated locking of $Tyr^{7.53}$ in one conformation, which was fully released only upon $Asp^{2.50}$-protonation (Fig. 3D), decoupled information exchange between $Tyr^{7.53}$ and the DRY motif.

Additionally, $Pro^{5.50}$ of the $P^{5.50}$-I-F motif also showed zero entropy, i.e. confinement to a single conformation, for the sodium-bound state. As opposed to protonation, SSI also indicated that sodium exerted an influence on both $I^{3.40}$ and $F^{6.44}$ of this motif. This highlighted that sodium altered the conformation of the P-I-F motif, which is known to be strongly coupled to ligand binding (24), as $F^{6.44}$ directly interacts with $W^{6.48}$, forming the base of the extracellular ligand binding pocket (37). By contrast, our entropy analysis revealed that all microswitches displayed fluctuations between various different conformational states in the sodium-free ($0/D^-$) simulations. In the protonated $Asp^{2.50}$ state, only $Asn^{1.50}$ was restrained to a single conformation in its vicinity.

In summary, we conclude that the sodium ion holds the receptor in the inactive state by restraining the key microswitches $Asp^{2.50}$, $Tyr^{7.53}$, $Asn^{1.50}$, and $Pro^{5.50}$ to single conformations. As they are locked in specific states, these microswitches are unable to participate in information transfer, disconnecting the information transfer route across the receptors that emerges fully only upon $Asp^{2.50}$ protonation. Since sodium dissociation is strongly coupled to $Asp^{2.50}$ protonation (10), the sodium–$Asp^{2.50}$ pair forms a single interlinked switch, governing information flow in GPCRs.

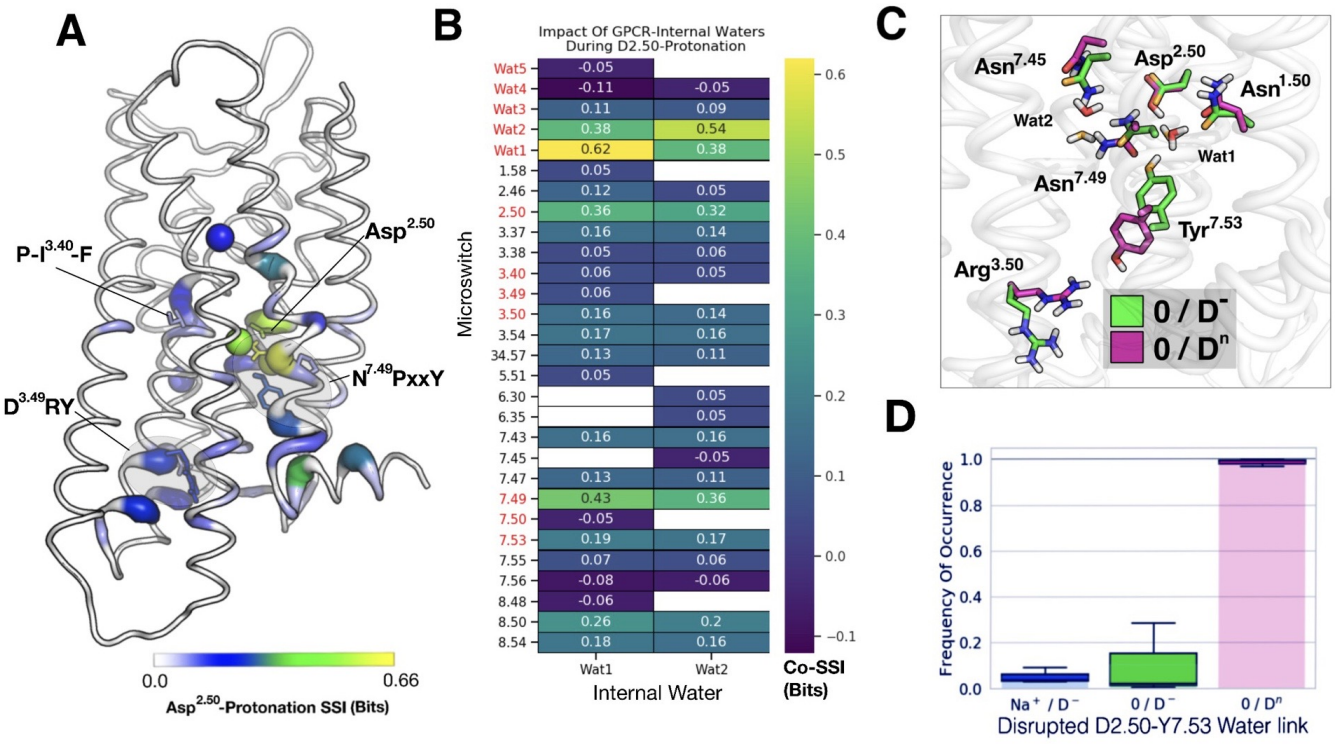

Fig. 3. Protonation establishes communication between NPxxY and DRY motifs by rotating water molecules. (A) SSI heatplot for Asp$^{2.50}$-protonation projected onto the μOR structure (pdb: 4dkl), highlighting information transfer with Asp$^{2.50}$. **(B)** Impact of the two water molecules, Wat1 and Wat2, on SSI transfer along the information pathway arising from Asp$^{2.50}$-protonation. Positive co-SSI values reveal that a water molecule (table columns) amplifies the information received by the microswitches (table rows) about Asp$^{2.50}$-protonation, whereas negative values reflect attenuation of information transmission. Protonation of Asp$^{2.50}$ unlocks new water states which allow them to amplify signal transfer along the channel. Co-SSI equals SSI when two out of three components are identical (e.g., Wat2, Wat2). Microswitch motifs and internal waters are highlighted in red. **(C)** Exemplar frames from molecular dynamics simulations of μOR in states 0/D$^-$ and 0/D^n; and **(D)** normalised count of water bridge formation between Asp$^{2.50}$ and Tyr$^{7.53}$ in all three Asp$^{2.50}$ states, averaged across the three receptors. For state 0/D$^-$, side chain carbon atoms are colored green and oxygen atoms (side chain and water) are coloured in orange. In state 0/D^n, carbon atoms are shown in magenta and oxygen atoms in red. The water bridge locks Tyr$^{7.53}$ in an upward-oriented state. Asp$^{2.50}$-protonation results in a rotation of water molecule Wat1 and the side chain conformation of Asn$^{7.49}$, leading to breakage of the water bridge in all three receptors. In the μOR, Tyr$^{7.53}$ then flips downwards, and Arg$^{3.50}$ moves upwards in concerted fashion, forming a water-mediated bond between the DR$^{3.50}$Y and NPxxY$^{7.53}$ motif.

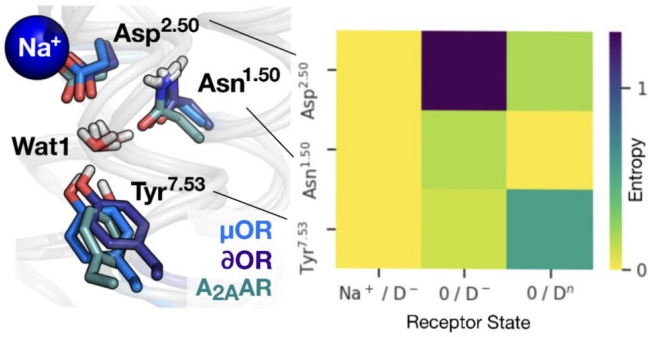

Fig. 4. Sodium confines Asp$^{2.50}$, Asn$^{1.50}$ and Tyr$^{7.53}$ to single conformations. Exemplar frames from molecular dynamics simulations of μOR, δOR and A_{2A}AR in the Na$^+$/D$^-$ state (left). The side chain conformational state entropy (right) of the sodium-bound conformations of Asp$^{2.50}$, Asn$^{1.50}$ and Tyr$^{7.53}$ is decreased to zero in all three receptors, fixing each residue to a specific conformation. All three residues participate in hydrogen bonding with Wat1 in the sodium-bound state, which correlates with a maintained water bridge between Asp$^{2.50}$ and Tyr$^{7.53}$ in all three receptors.

Discussion

Ions play important roles in GPCR signal transduction, affecting both their signal bias (38) and receptor activation (4, 8, 10, 36). In particular, a sodium ion bound to a highly conserved ionizable binding site (4, 5, 9, 13, 36) is known to play a key part in activating class A GPCRs. Signal transmission is further thought to be underpinned by a tightly connected network of polar residues and internal water molecules that extends across the receptors (14, 18) and by the conformational changes of protein microswitches (1, 17, 24). How these components interact to affect activation and signaling, however, has been unclear. Here, we applied information theory to μs-timescale simulations of three class A GPCRs to identify coupled transitions between these elements and examine their relation to receptor activation. Our results revealed that a long range information transfer pathway connects the most highly-conserved protonatable residues in class A GPCRs (Asp$^{2.50}$, Arg$^{3.50}$ and Asp$^{3.49}$) from the extracellular ion binding site to the intracellular G-protein interface (Fig. 5). The connectivity was established by protonation of Asp$^{2.50}$, triggered by the removal of a sodium ion that is known to bind to Asp$^{2.50}$ in the inactive receptor state (1, 8).

A network of ionizable residues extending through GPCRs is

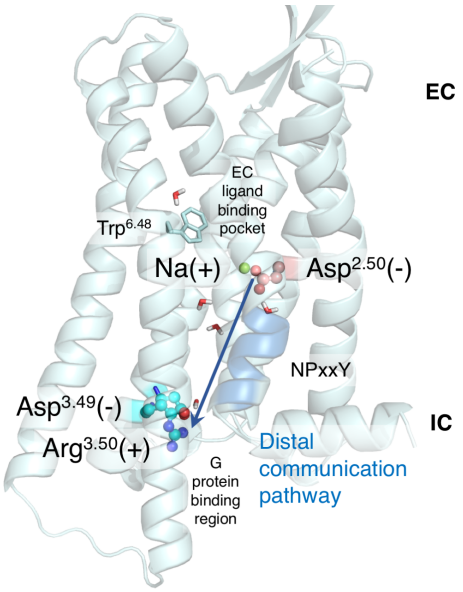

Fig. 5. A long range information transfer pathway connects the conserved ionizable rsidues $Asp^{2.50}$, $Arg^{3.50}$ and $Asp^{3.49}$, from the extracellular ion binding site to the intracellular G-protein interface. This allows protonatable sites at the G-protein interface regions to receive information about the $Asp^{2.50}$ protonation state, and implicates $Asp^{2.50}$ protonation in G-protein binding. EC, extracellular; IC, intracellular.

thought to be involved in GPCR signal transduction and may represent an evolutionary link to microbial rhodopsins (7, 10–13). Our findings therefore suggest that the long-range information pathway we identified may couple the protonation states of the distal conserved $Asp^{2.50}$ and $Arg^{3.50}$/$Asp^{3.49}$.

In the sodium-independent, visual class A GPCR rhodopsin, two protonation switches are known to initiate activation. The first protonation event is associated with the light-induced transition of the retinal Schiff base, central to the receptor similar to $Asp^{2.50}$ in non-visual receptors, while the additional protonation occurs at the $D^{3.49}$RY motif (39, 40). The coordinated action of such a conserved twin-protonation switch during activation of class A GPCRs would likely require a mechanism to relay protons, and exchange information about the states of the two distal sites. The information pathway we found between $Asp^{2.50}$ and $D^{3.49}$ is composed of polarizable water molecules and residues with conformations that couple to hydrogen bonding patterns at $Asp^{2.50}$, and therefore well suited to underpin proton transfer.

In many cases, ligand binding alone is thought to provide insufficient energy for receptors to transition between inactive and active conformations (7, 36). However, GPCRs are able to harness energy from the membrane potential gradient, potentially through ion and proton transfer (7, 10, 12, 41). Even in the presence of bound antagonists, we observed conformational rearrangements within highly conserved microswitches in the DRY and NPxxY motifs upon protonation of three receptors, which were reminiscent of the transition between inactive and active state crystal structures. This stochastic, ligand-independent sampling of active state conformations is in line with reports that suggest spontaneous $Asp^{2.50}$-protonation and egress of the sodium ion may be linked to basal signalling (10), as well as the observation that active state structures exhibit no bound sodium (8). Our results suggest that sodium unbinding and protonation, potentially coordinated between multiple conserved protonatable sites, play a key role in the activation process of class A receptors.

Two water molecules, structurally conserved across both active and inactive receptor states, are known to facilitate water-mediated interactions that correlate with the inactive (water 1) and active (water 2) receptor states (14). We found that these two water molecules function as microswitches which couple to the ion binding states of $Asp^{2.50}$. Both waters are essential for the transmission of information along a conserved pathway between the ion binding site and the DRY motif. Other water molecules play further important roles in connecting protein microswitch states over long ranges. By disabling protonation and tightly restraining the conformation of $Asp^{2.50}$ and neighboring residues, sodium stabilised the inactive state of the receptor and disconnected these information transfer pathways.

Only a small fraction of class A GPCRs do not possess a sodium binding site in their transmembrane domain (for example the NK1 neurokinin receptor (8, 42)), however they contain a similarly dense internal network of polar residues and water. Whereas $Asp^{2.50}$ is replaced by Glu, the DRY motif is still present in these receptors. A sodium-independent mechanism of switching protonation states and rearranging the polar network is conceivable in these cases. However, future studies will be necessary to confirm if the polar signal transmission and activation mechanism we find is conserved in the limited number of atypical class A GPCRs.

Materials and Methods.

Information Theory. The current consensus in the field is that slow modes in protein dynamics, for instance those of GPCR microswitches, have the greatest functional relevance, as they represent large scale changes between conformational states, rather than high frequency oscillations of the same conformational state (43). Therefore, in order to obtain mutual information between low frequency changes to microswitch rotamers, our methodology, State Specific Information (SSI), differs from traditional approaches that derive mutual information from atom or residue covariance during MD simulations (30, 32, 33, 44). In SSI, residue side chains are required to have at least two conformational states to store any information, e.g. 'up' and 'down' in the simplest case. By looking at the state of one residue, we can infer about the state of another, forming the first element of an information pathway. Deriving mutual information from long-lived conformational states rather than residue fluctuations eliminates noise from co-varying residues that always occupy the same conformation, while highlighting residues that are conformationally linked.

The analysis was divided into two pairwise combinations of the three ion binding states of $Asp^{2.50}$, isolating the functional effect of removing sodium from that of protonating $Asp^{2.50}$. Since we aimed to investigate the effect of sodium and protonation, isolated from any other ligand-induced ef-

fects, the antagonist bound to the inactive receptor state was added to every simulation. In this way, we focused on residue (and water) configurational changes that can be traced back to a certain cause, as opposed to pure correlative measures. The pairwise combinations of simulations were concatenated to create one larger trajectory representing the change in state of $Asp^{2.50}$: removal of sodium (sodium-bound $Asp^{2.50}$ [Na^+/D^-] + charged $Asp^{2.50}$ [0/D^-]), and protonation of $Asp^{2.50}$ (charged $Asp^{2.50}$ [0/D^-] + protonated $Asp^{2.50}$ [0/D^n]). Protonation is hypothesised to occur at the ion binding site during sodium removal and activation (10). The 'source information', which corresponded to the cause of the associated conformational changes, depended on the pairwise combination of simulations used, and represented the binary change made to the state of the ion binding site (i.e., 1 bit of information – sodium-bound to sodium-free; and sodium-bound or -free to protonated). The theoretical upper limit for all mutual and co-information values was therefore 1 bit. By assigning binary states to the two parts of the concatenated simulations representing the ion binding/protonation state, we were able to conclude whether sodium expulsion and protonation *caused* information to be shared between the ion binding site and any particular microswitch. For example, if information was shared between the states of the ion binding site and $Asn^{7.49}$, causality can be inferred because the state of the ion binding site can alter $Asn^{7.49}$, whereas the state of $Asn^{7.49}$ can not alter the ion binding site as it is constant throughout each simulation. The information transfer we resolve therefore only travels from the ion binding site, and not to the ion binding site, though in principle as SSI is symmetric then two-way transfer is possible.

We investigated all residues from the intracellular face to the base of the orthosteric pocket, including the CWxP motif. To focus on information pathways shared between all three receptors, residues whose Ballesteros-Weinstein positions were not common to all three receptors were omitted (for example in loops with differing lengths). Furthermore, we excluded Ballesteros-Weinstein positions that did not have variable side chain dihedral angles in the same position in all three receptors, resulting in a total of 121 investigated side chains. We then took the geometric mean of our results across all common Ballesteros-Weinstein positions. Residues whose configurations are dependent on the state of $Asp^{2.50}$ responded with distinct changes in their rotamer states. Additionally, by investigating the water occupancy and dynamics of a number of water sites conserved in both inactive and active state crystal structures, we quantified the influence of water on these communication pathways using co-information (also termed interaction information (30)), applied to residue states as co-SSI. There are different interpretations of negative co-information values in the literature (29–31). We adpoted the interpretation used by LeVine & Weinstein (30).

Residue side chain rotamer conformations were defined by in-house Gaussian style clustering to $\chi1$ and $\chi2$ dihedral angles, as seen in Fig. 6. A Hanning window function was used to smooth the probability density function to remove noise and locate the state maxima for each rotamer conformation. Guess parameters for Gaussian fitting were then obtained by locating the full-width at half-maximum from each maximum and Gaussian curve fitting was applied. The microswitch conformational state limits were defined as the Gaussian intersects. Each discretized distribution was additionally checked visually to ensure the fitting was accurate.

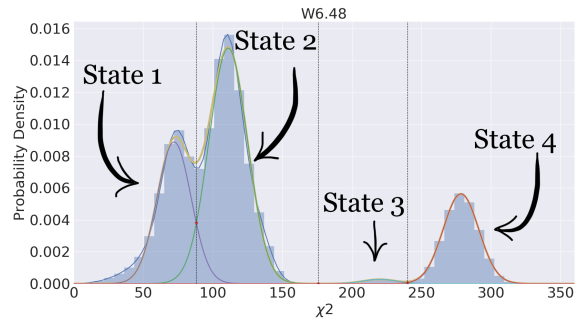

Fig. 6. Illustration of the Gaussian clustering method employed for defining discrete residue rotamer states. The example given is for the $\chi2$ angle of the highly conserved tryptophan residue $Trp^{6.48}$.

The dipole moment vector of water molecules (μ) was calculated by $\mu = 0.5(H_1 + H_2) - O$, where H_i is the (x,y,z) coordinate of the ith hydrogen, and O is the (x,y,z) coordinate of the oxygen. The orientation of water polarisation was calculated by converting the dot product of the dipole vector with the simulation box axes vectors into spherical coordinates, $\psi = arctan(\frac{y}{x})$ and $\theta = arctan\frac{\sqrt{x^2+y^2}}{z}$, followed by the same Gaussian style clustering algorithm.

When water was not found in a specific water pocket at a certain time point, that pocket was assigned an empty state. Water pockets must have had all three water atoms within the pocket as defined above to be considered occupied. Together, this allowed us to deduce the functional effect of each water pocket on the communication between microswitch pairs.

The conformational state entropy was determined from $H = -\sum_i p(i) log_2 p(i)$, where $p(i)$ is the probability of state i occurring, and H is the entropy, which is also a measure of the maximum information a microswitch can store. A regular average was taken across all common Ballesteros-Weinstein positions in the three receptors to deduce the average entropy of a specific residue. To stay consistent with the definition of states used in the state specific information transfer, the microswitch state limits of the concatenated simulations were used to define the states for the individual simulations. This ensured that residues would show zero entropy if they occupied only one of the information transfer states, and not just a single Gaussian distribution that spanned two information states, thereby identifying the effect of a specific $Asp^{2.50}$ state on the information states of the microswitch.

State Specific Information (SSI) between two residues X and Y was calculated using $SSI(X,Y) = H(X) + H(Y) - H(X,Y)$, where $H(X,Y)$ is the joint entropy (26), quantifying the entropy of the rotameric state of residues X and Y as one multivariate system. SSI is thereby a measure of the mutual information between discrete residue states.

The co-information (or interaction information), co-SSI, was

calculated using

$$
\begin{aligned}
coSSI(X,Y,H_2O) &= SSI(X,Y) - SSI(X,Y|H_2O) \\
&= H(X) + H(Y) + H(H_2O) \\
&- H(X,Y) - H(X,H_20) - H(Y,H_2O) \\
&+ H(X,Y,H_2O)
\end{aligned}
$$

where $SSI(X,Y|H_2O)$ determines what magnitude of SSI, or mutual information, shared between X and Y is dependent on the state of a specific third component, often an intercalating water molecule (H_2O) (28). We deemed SSI and co-SSI values of less than 0.05 bits insignificant on a 95% significance level.

Protein structure preparations. All crystal structures (μOR - pdb:4dkl, δOR - pdb:4n6h, A_{2A}AR - pdb:5olz) were obtained from GPCRdb (45), selecting the GPCRdb refined structure in which mutations are reversed to the canonical sequence and cleaved loops are re-modelled using MODELLER 9.18 to produce the final structure (46, 47). All transmembrane crystalline waters and ligands were kept in the structure, removing all external waters and non-protein molecules. The proteins were truncated and capped with acetyl and methyl groups at corresponding N and C terminals using PyMOL (48). As the μOR crystal structure did not resolve a sodium ion in the pocket, the sodium-bound structure was obtained by aligning the δOR crystal structure and placing the sodium ion in an identical position. $Asp^{2.50}$-charged protein structures were prepared by removing sodium from the crystal structure and ensuring no sodium ion re-associated during the course of the simulation. The third, protonated-$Asp^{2.50}$ protein state was prepared in the molecular dynamics software GROMACS-5.1.1 (49). Ligand structures were taken from their respective protein pdb files, and parameterised for molecular dynamics simulations in GROMACS-5.1.1 using ACPYPE (50).

MD simulations. We modelled the protein, membrane, and ligand using the amber99sb-ildn forcefield (51) in GROMACS-5.1.1 with virtual sites to allow a time-step of 4 fs. The proteins were embedded in a pre-equilibrated SLipid POPC membrane (52) using InflateGRO (53). The protein-membrane complexes were solvated with a neutral solution of TIP3P water molecules (54) containing NaCl at $\sim$150 mM concentration, with a box size of $\sim$128x134x125 $Å^3$. The systems were equilibrated in both the NVT and NPT ensembles at 310 K for 3 ns, with a further 70 ns of production run simulation considered as additional NPT equilibration. Following equilibration, simulations were performed for 1.7 μs each at a constant temperature of 310 K and pressure of 1 bar, with the protein-ligand complex, membrane, and solution independently coupled to a temperature bath using a Nosé-Hoover thermostat with a time constant of 0.5 ps and a semi-isotropic Parrinello-Rahman barostat with a time constant of 5 ps (55). The trajectory of the δOR protonated at $Asp^{2.50}$ was obtained from a previous simulation study (41, 56). All protein and lipid bond lengths were constrained with the LINCS algorithm (57), while water bond lengths were constrained using SETTLE (58).

Obtaining rotamer angles. Rotamer angles were determined every 240 ps using gmx_chi. The frame separation was chosen to be slightly smaller than the autocorrelation time of the conserved water dynamics with the fastest relaxation time (59). For μOR, water pockets were defined using MDAnalysis (60) as spheres of radius 4 Å centred on the geometric centres of (i) the tetrahedron formed by joining the C-α atoms of $Asn^{1.50}$-$Asp^{2.50}$-$Asn^{7.49}$-$Leu^{2.46}$; (ii) the triangle formed by joining the C-α atoms of $Asn^{7.45}$-$Asn^{7.49}$-$Ala^{6.38}$; (iii) the triangle formed by joining the C-α atoms of $Cys^{6.47}$-$Pro^{6.50}$-$Cys^{7.37}$; and (iv,v) spheres of 5 Å radius centred on the geometric centres of the tetrahedron formed by joining the C-α atoms of $Asn^{2.45}$-$Thr^{3.42}$-$Val^{4.45}$-$Trp^{4.50}$, and the triangle $Val^{3.48}$-$Arg^{34.57}$-$Ala^{4.42}$, respectively, as seen in Fig. 7. Similar positions were used for the δOR and A_{2A}AR, determined by centering the water probability density in the geometric centre of the selected C-α atoms.

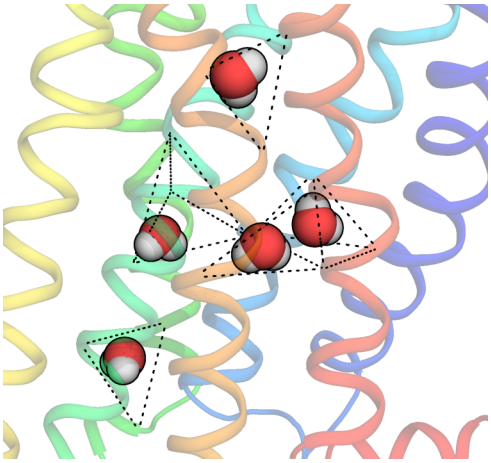

Fig. 7. Water pockets conserved in active and inactive crystal structures of μOR, A_{2A}AR and δOR. Pockets are defined as spheres of radii 4 Å and 5 Å centred on the centre of geometry of the respective triangles and tetrahedrons.

SUPPLEMENTARY MATERIALS

Fig. S1: $Asp^{2.50}$-protonation SSI.
Fig. S2: Sodium Expulsion SSI.
Fig. S3: Inter-hydroxyl distance between Tyr5.58-Tyr7.53 of μOR.
Fig. S4: Activation coordinate (TM2-TM6) in the δOR.
Fig. S5: $Asp^{2.50}$-protonation co-SSI For Wat1.
Fig. S6: $Asp^{2.50}$-protonation co-SSI For Wat2.
Fig. S7: $Asp^{2.50}$-protonation co-SSI For Wat3.
Fig. S8: $Asp^{2.50}$-protonation co-SSI For Wat4.
Fig. S9: $Asp^{2.50}$-protonation co-SSI For Wat5.
Fig. S10: Sodium Expulsion co-SSI For Wat1.
Fig. S11: Sodium Expulsion co-SSI For Wat2.
Fig. S12: Sodium Expulsion co-SSI For Wat3.
Fig. S13: Sodium Expulsion co-SSI For Wat4.
Fig. S14: Sodium Expulsion co-SSI For Wat5.

Bibliography

1. Vsevolod Katritch, Vadim Cherezov, and Raymond C Stevens. Structure-Function of the G Protein–Coupled Receptor Superfamily. *Annual Review of Pharmacology and Toxicology*, 53(1):531–556, 2013. doi: 10.1146/annurev-pharmtox-032112-135923.
2. Alexander S Hauser, Sreenivas Chavali, Ikuo Masuho, Leonie J Jahn, Kirill A Martemyanov, David E Gloriam, and M Madan Babu. Pharmacogenomics of GPCR Drug Targets. *Cell*, 172(1):41 – 54.e19, 2018. ISSN 0092-8674. doi: https://doi.org/10.1016/j.cell.2017.11.033.
3. Vignir Isberg, Chris de Graaf, Andrea Bortolato, Vadim Cherezov, Vsevolod Katritch, Fiona H Marshall, Stefan Mordalski, Jean-Philippe Pin, Raymond C Stevens, Gerrit Vriend, and David E Gloriam. Generic GPCR residue numbers – aligning topology maps while

minding the gaps. *Trends in Pharmacological Sciences*, 36(1):22–31, 2015. ISSN 0165-6147. doi: https://doi.org/10.1016/j.tips.2014.11.001.

4. Yinglong Miao, Alisha D Caliman, and J Andrew McCammon. Allosteric effects of sodium ion binding on activation of the m3 muscarinic g-protein-coupled receptor. *Biophysical journal*, 108(7):1796–1806, apr 2015. ISSN 1542-0086. doi: 10.1016/j.bpj.2015.03.003.
5. Libin Ye, Chris Neale, Adnan Sljoka, Brent Lyda, Dmitry Pichugin, Nobuyuki Tsuchimura, Sacha T Larda, Régis Pomès, Angel E García, Oliver P Ernst, et al. Mechanistic insights into allosteric regulation of the a 2a adenosine g protein-coupled receptor by physiological cations. *Nature communications*, 9(1):1–13, 2018.
6. Kate L. White, Matthew T. Eddy, Zhan Guo Gao, Gye Won Han, Tiffany Lian, Alexander Deary, Nilkanth Patel, Kenneth A. Jacobson, Vsevolod Katritch, and Raymond C. Stevens. Structural Connection between Activation Microswitch and Allosteric Sodium Site in GPCR Signaling. *Structure*, 26(2):259–269.e5, 2018. ISSN 18784186. doi: 10.1016/j.str.2017.12.013.
7. Daria N Shalaeva, Dmitry A Cherepanov, Michael Y Galperin, Gert Vriend, and Armen Y Mulkidjanian. G protein-coupled receptors of class A harness the energy of membrane potential to increase their sensitivity and selectivity. *Biochimica et Biophysica Acta (BBA) - Biomembranes*, 1861(12):183051, 2019. ISSN 0005-2736. doi: https://doi.org/10.1016/j.bbamem.2019.183051.
8. Barbara Zarzycka, Saheem A. Zaidi, Bryan L. Roth, and Vsevolod Katritch. Harnessing ion-binding sites for GPCR pharmacology. *Pharmacological Reviews*, 71(4):571–595, 2019. ISSN 15210081. doi: 10.1124/pr.119.017863.
9. Anirudh Ranganathan, Ron O Dror, and Jens Carlsson. Insights into the Role of Asp792.50 in β2 Adrenergic Receptor Activation from Molecular Dynamics Simulations. *Biochemistry*, 53(46):7283–7296, nov 2014. ISSN 0006-2960. doi: 10.1021/bi5008723.
10. Owen N Vickery, Catarina A Carvalheda, Saheem A Zaidi, Andrei V Pisliakov, Vsevolod Katritch, and Ulrich Zachariae. Intracellular Transfer of Na+ in an Active-State G-Protein-Coupled Receptor. *Structure*, 26(1):171 – 180.e2, 2018. ISSN 0969-2126. doi: https://doi.org/10.1016/j.str.2017.11.013.
11. Daniel G. Isom, Vishwajith Sridharan, Rachael Baker, Sarah T. Clement, David M. Smalley, and Henrik G. Dohlman. Protons as second messenger regulators of G protein signaling. *Molecular Cell*, 2013. ISSN 10972765. doi: 10.1016/j.molcel.2013.07.012.
12. Xuejun C Zhang, Can Cao, Ye Zhou, and Yan Zhao. Proton transfer-mediated GPCR activation. *Protein & Cell*, 6(1):12–17, 2015. ISSN 1674-8018. doi: 10.1007/s13238-014-0106-4.
13. Daniel G. Isom and Henrik G. Dohlman. Buried ionizable networks are an ancient hallmark of G protein-coupled receptor activation. *Proceedings of the National Academy of Sciences of the United States of America*, 2015. ISSN 10916490. doi: 10.1073/pnas.1417888112.
14. A J Venkatakrishnan, Anthony K Ma, Rasmus Fonseca, Naomi R Latorraca, Brendan Kelly, Robin M Betz, Chaitanya Asawa, Brian K Kobilka, and Ron O Dror. Diverse GPCRs exhibit conserved water networks for stabilization and activation. *Proceedings of the National Academy of Sciences*, 116(8):3288–3293, 2019. ISSN 0027-8424. doi: 10.1073/pnas.1809251116.
15. A. J. Venkatakrishnan, Xavier Deupi, Guillaume Lebon, Franziska M. Heydenreich, Tilman Flock, Tamara Miljus, Santhanam Balaji, Michel Bouvier, Dmitry B. Veprintsev, Christopher G. Tate, Gebhard F.X. Schertler, and M. Madan Babu. Diverse activation pathways in class A GPCRs converge near the G-protein-coupling region. *Nature*, 536:484–487, 2016. doi: 10.1038/nature19107.
16. Shuguang Yuan, Slawomir Filipek, Krzysztof Palczewski, and Horst Vogel. Activation of G-protein-coupled receptors correlates with the formation of a continuous internal water pathway. *Nature Communications*, 5(4733), 2014. ISSN 20411723. doi: 10.1038/ncomms5733.
17. Vsevolod V Gurevich and Eugenia V Gurevich. Molecular Mechanisms of GPCR Signaling: A Structural Perspective. *International journal of molecular sciences*, 18(12), nov 2017. ISSN 1422-0067. doi: 10.3390/ijms18122519.
18. Leonardo Pardo, Xavier Deupi, Nicole Dölker, María Luz López-Rodríguez, and Mercedes Campillo. The Role of Internal Water Molecules in the Structure and Function of the Rhodopsin Family of G Protein-Coupled Receptors. *ChemBioChem*, 8(1):19–24, jan 2007. ISSN 1439-4227. doi: 10.1002/cbic.200600429.
19. Yoonji Lee, Sun Choi, and Changbong Hyeon. Mapping the intramolecular signal transduction of G-protein coupled receptors. *Proteins: Structure, Function and Bioinformatics*, 82 (5):727–743, 2014. ISSN 10970134. doi: 10.1002/prot.24451.
20. Yoonji Lee, Sun Choi, and Changbong Hyeon. Communication over the Network of Binary Switches Regulates the Activation of A2A Adenosine Receptor. *PLoS Computational Biology*, 11(2):1–21, 2015. ISSN 15537358. doi: 10.1371/journal.pcbi.1004044.
21. B Trzaskowski, D Latek, S Yuan, U Ghoshdastider, A Debinski, and S Filipek. Action of molecular switches in GPCRs–theoretical and experimental studies. *Current medicinal chemistry*, 19(8):1090–1109, 2012. ISSN 1875-533X. doi: 10.2174/092986712799320556.
22. Katsufumi Tomobe, Eiji Yamamoto, Kholmirzo Kholmurodov, and Kenji Yasuoka. Water permeation through the internal water pathway in activated GPCR rhodopsin. *PLoS ONE*, 12(5):e0176876, 2017. ISSN 19326203. doi: 10.1371/journal.pone.0176876.
23. Qingtong Zhou, Dehua Yang, Meng Wu, Yu Guo, Wanjing Guo, Li Zhong, Xiaoqing Cai, Antao Dai, Wonjo Jang, Eugene Shakhnovich, Zhi Jie Liu, Raymond C. Stevens, Nevin A. Lambert, M. Madan Babu, Ming Wei Wang, and Suwen Zhao. Common activation mechanism of class a GPCRs. *eLife*, 8(e50279), 2019. ISSN 2050084X. doi: 10.7554/eLife.50279.
24. Oliver Fleetwood, Pierre Matricon, Jens Carlsson, and Lucie Delemotte. Energy landscapes reveal agonist control of g protein-coupled receptor activation via microswitches. *Biochemistry*, 59(7):880–891, 2020.
25. I. Rodriguez-Espigares, M. Torrens-Fontanals, J.K.S. Tiemann, et al. Gpcrmd uncovers the dynamics of the 3d-gpcrome. *Nature Methods*, 2020. doi: 10.1038/s41592-020-0884-y.
26. C E Shannon. A Mathematical Theory of Communication. *Bell System Technical Journal*, 27(3):379–423, 1948. doi: 10.1002/j.1538-7305.1948.tb01338.x.
27. Giovanni B Brandani, Marieke Schor, Cait E MacPhee, Helmut Grubmüller, Ulrich Zachariae, and Davide Marenduzzo. Quantifying disorder through conditional entropy: an application to fluid mixing. *PloS one*, 8(6):e65617, 2013.
28. W. McGill. Multivariate information transmission. *Transactions of the IRE Professional Group on Information Theory*, 4(4):93–111, 1954.
29. Anthony J Bell. The co-information lattice. In *Proceedings of the Fifth International Workshop on Independent Component Analysis and Blind Signal Separation: ICA*, volume 2003. Citeseer, 2003.
30. Michael V LeVine and Harel Weinstein. NbIT - A New Information Theory-Based Analysis of Allosteric Mechanisms Reveals Residues that Underlie Function in the Leucine Transporter LeuT. *PLOS Computational Biology*, 10(5):1–15, 2014. doi: 10.1371/journal.pcbi.1003603.
31. A Ghassami and N Kiyavash. Interaction information for causal inference: The case of directed triangle. In *2017 IEEE International Symposium on Information Theory (ISIT)*, pages 1326–1330, 2017. ISBN 2157-8117 VO -. doi: 10.1109/ISIT.2017.8006744.
32. Abhijeet Kapoor, Gerard Martinez-Rosell, Davide Provasi, Gianni de Fabritiis, and Marta Filizola. Dynamic and Kinetic Elements of μ-Opioid Receptor Functional Selectivity. *Scientific Reports*, 7(1):11255, 2017. ISSN 2045-2322. doi: 10.1038/s41598-017-11483-8.
33. Aysima Hacisuleyman and Burak Erman. Entropy Transfer between Residue Pairs and Allostery in Proteins: Quantifying Allosteric Communication in Ubiquitin. *PLOS Computational Biology*, 13(1):1–23, 2017. doi: 10.1371/journal.pcbi.1005319.
34. Nuray Sogunmez and Ebru Demet Akten. Distinctive communication networks in inactive states of β2-adrenergic receptor: Mutual information and entropy transfer analysis. *Proteins: Structure, Function and Bioinformatics*, 2020. ISSN 10970134. doi: 10.1002/prot.25965.
35. Kateri H. DuBay, Jacques P. Bothma, and Phillip L. Geissler. Long-range intra-protein communication can be transmitted by correlated side-chain fluctuations alone. *PLoS Computational Biology*, 2011. ISSN 1553734X. doi: 10.1371/journal.pcbi.1002168.
36. Vsevolod Katritch, Gustavo Fenalti, Enrique E Abola, Bryan L Roth, Vadim Cherezov, and Raymond C Stevens. Allosteric sodium in class A GPCR signaling. *Trends in Biochemical Sciences*, 39(5):233–244, 2014. ISSN 0968-0004. doi: https://doi.org/10.1016/j.tibs.2014.03.002.
37. Edward C Hulme. GPCR activation: a mutagenic spotlight on crystal structures. *Trends in Pharmacological Sciences*, 34(1):67–84, jan 2013. ISSN 0165-6147. doi: 10.1016/j.tips.2012.11.002.
38. Jing Yu, Luis E Gimenez, Ciria C Hernandez, Yiran Wu, Ariel H Wein, Gye Won Han, Kyle McClary, Sanraj R Mittal, Kylie Burdsall, Benjamin Stauch, et al. Determination of the melanocortin-4 receptor structure identifies ca2+ as a cofactor for ligand binding. *Science*, 368(6489):428–433, 2020.
39. Mohana Mahalingam, Karina Martínez-Mayorga, Michael F Brown, and Reiner Vogel. Two protonation switches control rhodopsin activation in membranes. *Proceedings of the National Academy of Sciences*, 105(46):17795–17800, 2008. ISSN 0027-8424. doi: 10.1073/pnas.0804541105.
40. Udeep Chawla, Suchithranga Perera, Steven Fried, Anna Eitel, Blake Mertz, Nipuna Weerasinghe, Michael Pitman, Andrey Struts, and Michael F Brown. Activation of the G-Protein-Coupled Receptor Rhodopsin by Water. *Angewandte Chemie International Edition*, 2020. ISSN 1433-7851. doi: 10.1002/anie.202003342.
41. Owen N. Vickery, Jan-Philipp Machtens, Giulia Tamburrino, Daniel Seeliger, and Ulrich Zachariae. Structural Mechanisms of Voltage Sensing in G-Protein-Coupled Receptors. *Structure*, 24(6):997–1007, jun 2016. ISSN 0969-2126. doi: 10.1016/j.str.2016.04.007.
42. Jendrik Schöppe, Janosch Ehrenmann, Christoph Klenk, Prakash Rucktooa, Marco Schütz, Andrew S Doré, and Andreas Plückthun. Crystal structures of the human neurokinin 1 receptor in complex with clinically used antagonists. *Nature communications*, 10(1):1–11, 2019.
43. Naomi R Latorraca, A J Venkatakrishnan, and Ron O Dror. GPCR Dynamics: Structures in Motion. *Chemical Reviews*, 117(1):139–155, jan 2017. ISSN 0009-2665. doi: 10.1021/acs.chemrev.6b00177.
44. Oliver F Lange and Helmut Grubmüller. Generalized correlation for biomolecular dynamics. *Proteins: Structure, Function, and Bioinformatics*, 62(4):1053–1061, 2006. doi: 10.1002/prot.20784.
45. Vignir Isberg, Stefan Mordalski, Christian Munk, Krzysztof Rataj, Kasper Harpsøe, Alexander S. Hauser, Bas Vroling, Andrzej J. Bojarski, Gert Vriend, and David E. Gloriam. GPCRdb: An information system for G protein-coupled receptors. *Nucleic Acids Research*, 44(D1):D356–64, 2016. ISSN 13624962. doi: 10.1093/nar/gkv1178.
46. Benjamin Webb and Andrej Sali. Comparative Protein Structure Modeling Using MODELLER. *Current Protocols in Bioinformatics*, 54(1):5.6.1–5.6.37, 2016. doi: 10.1002/cpbi.3.
47. Gáspár Pándy-Szekeres, Christian Munk, Tsonko M Tsonkov, Stefan Mordalski, Kasper Harpsøe, Alexander S Hauser, Andrzej J Bojarski, and David E Gloriam. GPCRdb in 2018: adding GPCR structure models and ligands. *Nucleic Acids Research*, 46(D1):D440–D446, nov 2017. ISSN 0305-1048. doi: 10.1093/nar/gkx1109.
48. Warren L DeLano. Pymol: An open-source molecular graphics tool. *CCP4 Newsletter on protein crystallography*, 40(1):82–92, 2002.
49. Mark James Abraham, Teemu Murtola, Roland Schulz, Szilárd Páll, Jeremy C Smith, Berk Hess, and Erik Lindahl. GROMACS: High performance molecular simulations through multi-level parallelism from laptops to supercomputers. *SoftwareX*, 1-2:19–25, 2015. ISSN 2352-7110. doi: https://doi.org/10.1016/j.softx.2015.06.001.
50. Alan W Sousa da Silva and Wim F Vranken. ACPYPE - AnteChamber PYthon Parser interfacE. *BMC Research Notes*, 5(1):367, 2012. ISSN 1756-0500. doi: 10.1186/1756-0500-5-367.
51. Kresten Lindorff-Larsen, Stefano Piana, Kim Palmo, Paul Maragakis, John L Klepeis, Ron O Dror, and David E Shaw. Improved side-chain torsion potentials for the Amber ff99SB protein force field. *Proteins*, 78(8):1950–1958, jun 2010. ISSN 1097-0134. doi: 10.1002/prot.22711.
52. Joakim P M Jämbeck and Alexander P Lyubartsev. An Extension and Further Validation of an All-Atomistic Force Field for Biological Membranes. *Journal of Chemical Theory and Computation*, 8(8):2938–2948, aug 2012. ISSN 1549-9618. doi: 10.1021/ct300342n.
53. Christian Kandt, Walter L Ash, and D Peter Tieleman. Setting up and running molecular dynamics simulations of membrane proteins. *Methods*, 41(4):475–488, 2007. ISSN 1046-2023. doi: https://doi.org/10.1016/j.ymeth.2006.08.006.
54. William L Jorgensen, Jayaraman Chandrasekhar, Jeffry D Madura, Roger W Impey, and Michael L Klein. Comparison of simple potential functions for simulating liquid water. *The Journal of Chemical Physics*, 79(2):926–935, 1983. doi: 10.1063/1.445869.
55. Giovanni Bussi, Tatyana Zykova-Timan, and Michele Parrinello. Isothermal-isobaric molecular dynamics using stochastic velocity rescaling. *The Journal of Chemical Physics*, 130(7):

74101, feb 2009. ISSN 0021-9606. doi: 10.1063/1.3073889.
56. Owen N Vickery, Jan-Philipp Machtens, and Ulrich Zachariae. Membrane potentials regulating gpcrs: insights from experiments and molecular dynamics simulations. *Current Opinion in Pharmacology*, 30:44–50, 2016.
57. Berk Hess, Henk Bekker, Herman JC Berendsen, and Johannes GEM Fraaije. Lincs: a linear constraint solver for molecular simulations. *Journal of computational chemistry*, 18 (12):1463–1472, 1997.
58. Shuichi Miyamoto and Peter A Kollman. Settle: An analytical version of the shake and rattle algorithm for rigid water models. *Journal of computational chemistry*, 13(8):952–962, 1992.
59. Yoonji Lee, Songmi Kim, Sun Choi, and Changbong Hyeon. Ultraslow Water-Mediated Transmembrane Interactions Regulate the Activation of A2A Adenosine Receptor. *Biophysical journal*, 111(6):1180–1191, sep 2016. ISSN 1542-0086. doi: 10.1016/j.bpj.2016.08.002.
60. Naveen Michaud-Agrawal, Elizabeth J Denning, Thomas B Woolf, and Oliver Beckstein. MDAnalysis: A toolkit for the analysis of molecular dynamics simulations. *Journal of Computational Chemistry*, 32(10):2319–2327, jul 2011. ISSN 0192-8651. doi: 10.1002/jcc.21787.

ACKNOWLEDGEMENTS
We thank Seva Katritch for critical reading of the manuscript.

FUNDING
This work was supported by a BBSRC EASTBIO PhD studentship (to N.J.T.); a BBSRC Case award (to O.N.V.); and an MRC 4-year PhD studentship (to C.M.I.).

AUTHOR CONTRIBUTIONS
Conceptualization: N.J.T and U.Z. Methodology: N.J.T and U.Z. Formal analysis: N.J.T and U.Z. Investigation: N.J.T, O.N.V and U.Z. Writing (original draft): N.J.T and U.Z. Writing (review and editing): N.J.T, C.M.I and U.Z. Supervision: U.Z.

COMPETING INTERESTS
The authors declare that they have no competing interests.